Received: 3 October 2019 | Revised: 15 October 2019 | Accepted: 1 November 2019

DOI: 10.1002/hipo.23180

WILEY

RESEARCH ARTICLE

Hippocampal state transitions at the boundaries between trial epochs

David A. Bulkin[1] | David G. Sinclair[2] | L. Matthew Law[3,4] | David M. Smith[1]

[1]Department of Psychology, Cornell University, Ithaca, New York

[2]Department of Statistical Science, Cornell University, Ithaca, New York

[3]BARROW Neurological Institute at Phoenix Children's Hospital, Phoenix, Arizona

[4]Department of Child Health, University of Arizona College of Medicine, Phoenix, Arizona

Correspondence
David M. Smith, Department of Psychology, Cornell University, Ithaca, NY.
Email: dms248@cornell.edu

Funding information
National Institute of Mental Health, Grant/Award Number: R01 MH083809

Abstract

The hippocampus encodes distinct contexts with unique patterns of activity. Representational shifts with changes in context, referred to as remapping, have been extensively studied. However, less is known about transitions between representations. In this study, we leverage a large dataset of neuronal recordings taken while rats performed an olfactory memory task with a predictable temporal structure involving trials and intertrial intervals (ITIs), separated by salient boundaries at the trial start and trial end. We found that trial epochs were associated with stable hippocampal representations despite moment-to-moment variability in stimuli and behavior. Representations of trial and ITI epochs were far more distinct than spatial factors would predict and the transitions between the two were abrupt. The boundary was associated with a large spike in multiunit activity, with many individual cells specifically active at the start or end of each trial. Both epochs and boundaries were encoded by hippocampal populations, and these representations carried information on orthogonal axes readily identified using principal component analysis. We suggest that the hippocampus orthogonalizes representations of the trial and ITI epochs and the activity spike at trial boundaries might serve to drive hippocampal activity from one stable state to the other.

KEYWORDS
context, event segmentation, memory, remapping

1 | INTRODUCTION

For animals to successfully interact with their environment they need to construct neural representations that allow them to identify the current context and select appropriate behavioral responses, and they need to rapidly transition between these representations when the context changes. A large literature has suggested that hippocampal activity patterns represent the environmental context (Colgin, Moser, & Moser, 2008; Holland & Bouton, 1999; Nadel, 2008; Rudy, 2009) and we have shown that distinct hippocampal representations are essential for the ability to retrieve context-appropriate memories while avoiding interference from memories that belong to other contexts (Bulkin, Law, & Smith, 2016; Butterly, Petroccione, & Smith, 2012; Smith & Bulkin, 2014). The hippocampus has the capacity to generate many distinct representations (Alme et al., 2014) and the environmental factors that induce the formation of a new representation (i.e., remapping) have been studied extensively (Anderson & Jeffery, 2003; Colgin et al., 2008; Leutgeb et al., 2005; Leutgeb, Leutgeb, Moser, & Moser, 2007; Muller & Kubie, 1987; Schlesiger, Boublil, Hales, Leutgeb, & Leutgeb, 2018). Changes in the nonspatial characteristics of the context, such as behavioral demands, strategy and motivation, are also known to induce remapping (Eschenko & Mizumori, 2007; Ferbinteanu & Shapiro, 2003; Kennedy & Shapiro, 2009; Skaggs & McNaughton, 1998; Smith & Mizumori, 2006; Terrazas et al., 2005; Wood, Dudchenko, Robitsek, & Eichenbaum, 2000). Studies of hippocampal representations during context transitions have shown patterns that are rapid and abrupt, rather than a gradual progression through intermediate representations (Jezek,

Henriksen, Treves, Moser, & Moser, 2011; Kelemen & Fenton, 2010; Wills, Lever, Cacucci, Burgess, & O'Keefe, 2005). However, these studies often involve artificial experimental conditions unlike those commonly encountered in day-to-day experience (e.g., an unexpected and dramatic change in the visual environment, described as "teleportation" by Jezek et al. (2011)). Much less is known about more mundane and highly predictable changes in the context such as walking from the living room into the kitchen. Indeed, it is not clear whether the hippocampus treats contiguous spaces as distinct contexts and if so, how hippocampal representations transition from one to the other.

In this article, we leverage a large dataset of 2056 neurons recorded during a complex multistimulus olfactory discrimination task with two behaviorally and spatially distinct areas (a trial area and an intertrial waiting area) and a predictable trial structure to interrogate the dynamics of hippocampal representations. We discovered that hippocampal populations form two distinct representations of the trial and intertrial interval (ITI) epochs, and that the shift between these representations was accompanied by a surge of activity among subsets of hippocampal neurons. These firing patterns resembled a phase transition: the hippocampal state before trials transformed to a distinct state during trials, and then transformed back at the end of trials, with an identifiable transitory activity pattern between states.

2 | METHODS

2.1 | Surgical and recording methods

Rats were surgically implanted with custom-built moveable electrode arrays containing 16 insulated platinum iridium tetrodes, each composed of four 17 μm wires (California Fine Wire, Grover Beach, CA). Arrays were implanted with electrode tips located bilaterally just above the dorsal hippocampus (3.5 mm posterior and 2.5 mm lateral to bregma). Following recovery from surgery, the tetrodes were slowly lowered into the CA1 cell layer and rats began training on the behavioral task. Tetrodes were advanced over initial training and then left in place once rats reached asymptotic performance on the behavioral task. Multiunit recordings were sorted into constituent units using standard clustering techniques. We report on the activity of 2,056 units recorded from 10 rats over 84 sessions (see Supplementary Table S1), counting individual recordings of units recorded over sessions (i.e., some units refer to a single neuron that was recorded on multiple sessions). Field potentials were sampled at 32 kHz from one wire in each tetrode, and filtered between 0.1 and 6 kHz, a representative signal was chosen from a tetrode located in the cell layer. All procedures complied with the guidelines established by the Cornell University Animal Care and Use Committee.

2.2 | Behavioral procedure and apparatus

Ten adult male Long–Evans rats were trained on a task designed to induce proactive mnemonic interference. Details on the task and the relationship between hippocampal activity and interference have been described elsewhere (Bulkin et al., 2016; Butterly et al., 2012; Law & Smith, 2012; Peters, David, Marcus, & Smith, 2013). Recordings took place in wooden chambers with a 60×45 cm^2 floor and a removable divider (Figure 1a). One side of the chamber served as an intertrial waiting area, the other contained two cups filled with odorized digging substrate. One of the cups was baited with a buried sugar pellet, reliably marked by odor, and rats learned to discriminate between eight pairs of odors to retrieve rewards. The left and right position of the rewarded cup was randomized. On each trial, the divider was lifted, rats approached the cups and sampled odors, and dug for the sugar pellet. Rats were free to approach either cup first and they sometimes approached the baited cup first, simply by chance, and completely ignored the unbaited odor (Supplementary Figure S1b). Trials in which the rat sampled the unbaited odor and did not dig were marked as a correct rejection (Supplementary Figure S1c). Trials were marked as errors if the rat dug in the unbaited cup (Supplementary Figure S1d), any displacement of bedding was considered a digging response. Once the rat reached a behavioral criterion of 90% correct choices, a new set of odor pairs was presented, and training on this new set continued for 5 days. A subset of rats (N = 4) learned this new set in a distinct context and the results of manipulating the context on behavioral performance and hippocampal ensemble activity have been described previously (Bulkin et al., 2016). In that paper, we found that place fields and responses to the odor cues remapped with changes in context and the odor sets. In the present paper, we focused on the responses within each session at the start and end of trials and differences between the trial and ITI epochs. We also examined these firing patterns to determine whether they changed across learning, across the switch from the first odor set to the second, and across contexts. In contrast to the place fields and odor responses of our previous report, trial start/end firing patterns did not show clear or systematic changes across learning or contexts. Recordings were only taken on sessions with at least two units, although in most cases many more units were isolated: at least 10 units in 74/84 sessions (mean units/session 24.5; Supplementary Table S1 summarizes the number of units by rat/session).

2.3 | Data analysis

2.3.1 | Instantaneous firing rate

For each neuron, spike counts were binned across the entire session (100 ms bins) and smoothed with a 5-bin moving average to construct a vector of instantaneous firing rate (IFR). This trace was normalized by subtracting the average and dividing by the standard deviation (i.e., z-scored) to produce a normalized IFR (IFRz). Because units showed a similar range of activity, analyses showed qualitatively similar results when using IFR or IFRz, but the latter prevented neurons with higher overall firing rates from dominating the analyses. Units with average rates greater than four spikes/second over the entire session were labeled as putative interneurons, and were not included in any of the analyses (235/2,291 units were eliminated). Population

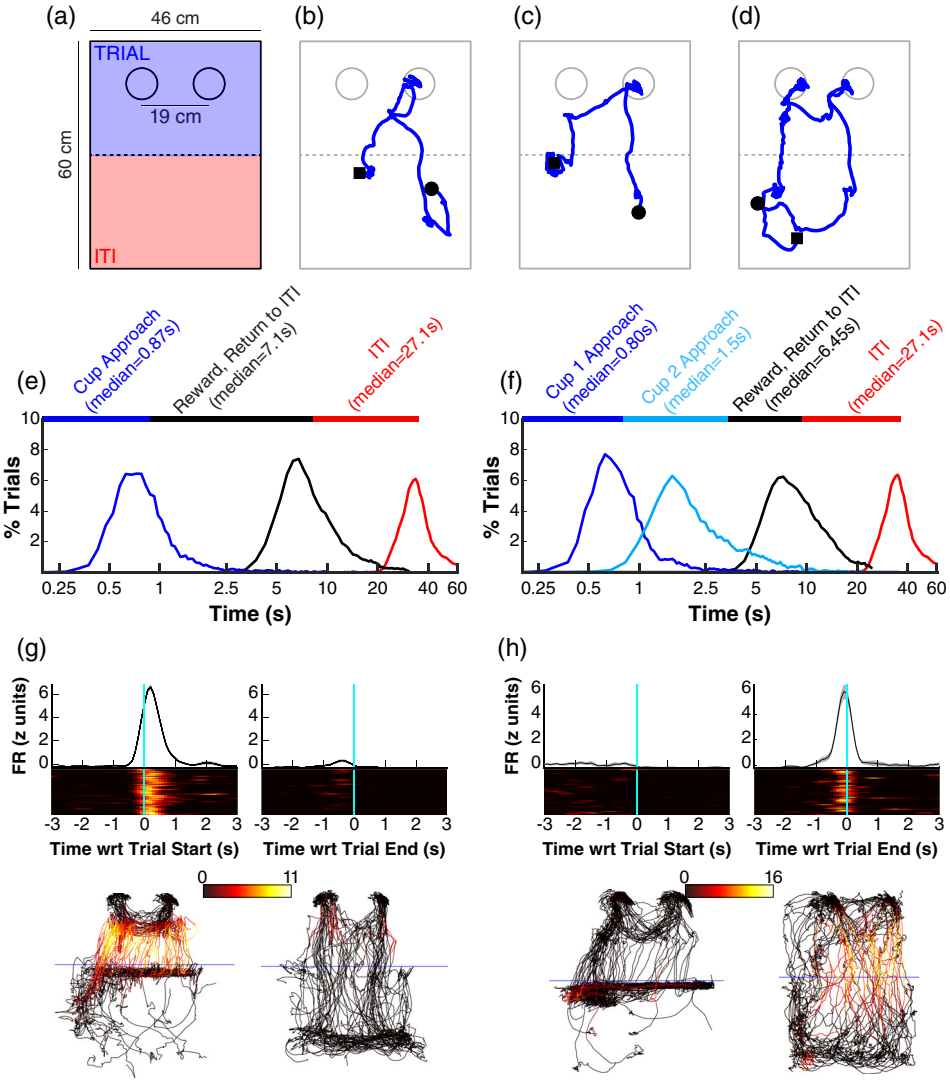

FIGURE 1 Reliable neuronal responses to the start and end of trials despite large variability in spatiotemporal patterns of behavior. Rats performed trials in 60 × 46 cm wooden boxes (a). The boxes were bisected by a removable divider (dotted line). One side of the box served as the intertrial waiting area, and rats performed trials in the other side. During the trials, rats dug for a reward buried in one of two cups, placed in cup holders indicated by the two circles. Panels (b)–(d) show example positional trajectories, beginning 3 s before the trial start (black squares) and extending 3 s after the trial end (black circles). (b) A trial where the rat first approached the cup on the right, which was the baited cup for this trial, and dug for a reward. (c) A trial where the rat approached and sampled the unbaited cup on the left, correctly rejected it, and then dug for a reward in the baited cup on the right. (d) is similar to (c), except that the rat made an error by digging in the cup on the left, but then approached the baited cup on the right and obtained the reward. Panels (e) and (f) illustrate the time line and variability in how the trials proceeded. The median time of arrival at the cup (blue), the time spent retrieving the reward and returning to the intertrial interval (ITI) side of the box (black), and the duration of the ITI (red) are indicated by the horizontal lines. The histograms illustrate the variability in the duration of these epochs. Panel (f) shows the same data for trials in which the rats approached both cups (i.e., trials with trajectories like those shown in (c) and (d)). Note the use of a log scale for the abscissa in (e) and (f). Panels (g) and (h) show data from an example trial start and trial end neuron. At the top, the average firing aligned on the start (left) and end (right) is shown. Below, a heatmap shows the firing on each trial. At the bottom, the trajectory of the rat is shown for a period matching the above plots, with color indicating the instantaneous firing rate (IFR) of the neurons. The horizontal line indicates the position of the divider [Color figure can be viewed at wileyonlinelibrary.com]

vectors (PVs) were defined as $n \times 1$ vectors of IFRz at a given time, where n is the number of simultaneously recorded neurons.

The start and end of trials were identified as the moment the rat crossed an imaginary line corresponding to the location of the removable divider. Generally, rats only crossed this line once in each direction on each trial, but on those trials in which the rat entered the trial region and then returned back to the intertrial waiting area only the first entry was used to mark the start of the trial. Trial start and end firing rate traces were calculated by linear interpolation of the IFR vector at times spanning ±3 s on the trial start and end. Spatial heatmaps were calculated by identifying the average firing rate of each neuron in 1.5 cm^2 bins spanning the floor of the apparatus.

2.3.2 | Local field potentials

The local field potential data was downsampled to 2 kHz. The theta–delta ratio was identified by filtering the signal (theta: 5–12 Hz; delta: 2–4 Hz) with a noncausal finite impulse response (FIR) filter, calculating root mean square (RMS) power with a 500 ms sliding window, and taking the quotient.

2.3.3 | Running speed

Running speed was computed by applying a 1 s boxcar average to position. Average firing rate was calculated for binned running speeds (15 bins) separately for times near the trial start and end (±1 s), in the trial (1 s after the start to 1 s before the end) and in the ITI (1 s after the trial end to 1 s before the trial start). A linear regression was calculated for data collected in each epoch to describe multiunit activity as a function of running speed. The slope and intercept of these regressions were compared for neurons showing a slope that was significantly different from 0 (F-test, $p < .01$).

2.3.4 | Generalized linear model

The strategy for applying a generalized linear model (GLM) that orthogonalized the contributions of spatial and temporal covariates was adapted from Truccolo, Eden, Fellows, Donoghue, and Brown (2004) and Lepage, MacDonald, Eichenbaum, and Eden (2012). This approach relies on a geometry in the Fisher information of the GLM likelihood estimator to disambiguate activity due to a combination of multiple covariates. Applying this method to two-dimensional spatial data required a parameterization of spatial firing functions as activity depends on an interaction between the x and y coordinates defining the rat's position. As such, we first described both the temporal and spatial firing rate by fitting Gaussian curves and surfaces to the average firing data:

$$f_{\text{space}}(x, y) = \beta_1 \left(e^{-\frac{(x-\mu_x)^2}{2\sigma_x^2} - \frac{(y-\mu_y)^2}{2\sigma_y^2}} \right) + C$$

$$f_{\text{start}}(t_s) = \beta_2 \left(e^{-\frac{(t_s-\mu_s)^2}{2\sigma_s^2}} \right) + C$$

$$f_{\text{end}}(t_e) = \beta_3 \left(e^{-\frac{(t_e-\mu_e)^2}{2\sigma_e^2}} \right) + C$$

We modeled the coefficients β_1, β_2, β_3 by fitting a Poisson family GLM with a linear link function. Given the rat's location (x, y), and the time relative to trial start (t_s) and end (t_e), the firing rate for each neuron was modeled as:

$$E(\text{FiringRate} \mid x, y, t_s, t_e) = f_{\text{space}}(x, y) + f_{\text{start}}(t_s) + f_{\text{end}}(t_e)$$

We also computed a model which included an additional factor for running speed:

$$f_{\text{runspeed}}(rs) = \beta_4(rs) + C$$

Because a linear link function in a Poisson GLM includes the possibility for negative rates, the β_1, β_2, β_3, β_4 parameters were restricted to be greater than or equal to 0. Since the true values could never be exactly zero, this does not break down the asymptotic orthogonalization results from Lepage et al. (2012). The restriction of the parameter space means that parameters estimated to be 0 would have a negatively biased standard error in comparison to the traditional Wald test and likelihood ratio tests for GLMs. For this reason, we instead used a normal approximation significance test adapted from the normal theory bootstrap intervals given in Efron and Tibshirani (1994) to test if each parameter was significantly different than 0. If the bootstrapped sample for a parameter contained more than 10% of values selected exactly at 0, then a quantile-based significance test was used (Efron & Tibshirani, 1994). The quantile-based significance test was used in this case as the normality assumption on the bootstrapped sample no longer holds; however, the quantile-based tests were not used across all observations to allow p-values to be calculated to more than three significant digits for significant parameters. The bootstrap was completed by randomly sampling 1 s blocks of data for each neuron with replacement. The blocking was done to account for the temporal dependencies in the data set (Gonçalves & Politis, 2011). Within each neuron, 250 bootstrap samples were created for each parameter in order to obtain a p-value. A significant effect was tabulated as any coefficient value with $p < .01$, for comparisons that grouped trial start and end responses together these p values were Bonferroni corrected.

2.3.5 | Cross-trial distance analysis

To compute cross-trial instantaneous ensemble firing rate similarity (Figure 3a–c), PVs of IFR were assembled for times spanning ±3 s in 100 ms intervals around each trial's start and end. For each time point in each trial, the pairwise correlation between the associated PV and all PVs from all other trials at each time point was calculated. The average of these values was taken for each rat to form a cross-trial correlation map for the session, each pixel representing the average correlation between PVs taken from two time points across all pairs of trials. Correlation was calculated using both Pearson's r and Kendall's τ.

2.3.6 | Classification of trial versus ITI responses

To identify the ability of neuronal populations to identify the current epoch, we trained linear discriminant classifiers to mark epoch based on activity. We first assembled PVs spanning ±3 s around the trial start and trial end, labeling each vector with the epoch in which it occurred. We took a random subset of half of these vectors and trained a linear discriminant classifier, separately for data occurring around the trial start or trial end, and tested the classifier on the remaining 50% of the data. This process was repeated 1,000 times, on

each iteration a different random subset was used to train/test the performance of the classifier. The overall performance of the classifier was measured as the median performance across iterations, and the fifth percentile of iterations was used to identify whether the classifier performed above chance.

2.3.7 | Principal component analysis

To investigate population dynamics at the start and end of trials across the entire dataset, we created a synthetic dataset by sampling activity from defined time points around the trial start and end. This allowed visualization of activity in coordinates scaled by key sources of variance across a large population of neurons. One strategy for forming this synthetic dataset would be to randomly select activity from each neuron at a given time with respect to the trial boundaries; however, this approach would randomize covariance between neurons. Instead, we selected vectors from each session, preserving information about interneuron covariance when possible (i.e., within session) and randomizing when covariance data was unavailable (i.e., across sessions).

For each recording session (ses), we constructed PVs ($\vec{PV}$) as the IFR at time points (t) spanning ±5 s around each trial's (trial) start and end in 100 ms intervals.

$$\underset{n\times 1}{\vec{PV}}(\text{ses},\text{trial},t)=\begin{bmatrix}x_1\\x_2\\\vdots\\x_n\end{bmatrix}$$

In the above equation, x_1 indicates the firing rate of neuron 1 from recording session ses, trial number trial at the time specified by t. For instance, $\vec{PV}(8,14,1)$ would contain the firing rates of all neurons recorded during Session 8, on Trial 14, 5.0 s before the trial start.

We then randomly selected a trial from each session and combined the PVs across sessions (ν = 84 total sessions), holding t constant, to form pseudo-PVs $\vec{PPV}$.

$$\vec{PPV}_{N\times 1}(\text{iter},t)=\begin{bmatrix}\vec{PV}(1,\text{rand},t)\\\vec{PV}(2,\text{rand},t)\\\vdots\\\vec{PV}(\nu,\text{rand},t)\end{bmatrix}$$

$\vec{PPV}$ contains the firing rate of all N neurons (N = 2,056), on randomly selected trial, at some specific time (t) with respect to the trial start or end. It indicates what an ensemble of N neurons might look like at a given time.

We repeated this process over 200 iterations, and over all time windows, to form a $N \times M$ matrix. Each column of the matrix contains an iteratively selected ensemble firing rate at some time with respect to trial start or end.

$$\text{PPM}_{N\times M}=\left[\overrightarrow{\text{PPV}}(1,1)\ \overrightarrow{\text{PPV}}(1,2)\cdots\overrightarrow{\text{PPV}}(1,n_{\text{iter}})\ \overrightarrow{\text{PPV}}(2,1)\cdots\overrightarrow{\text{PPV}}(n_t,n_{\text{iter}})\right]$$

The total number of columns of PPM, denoted as M, is the product of the number of iterations (n_{iter}) and the number of sampled time points (n_t):

$$M=n_{iter}\cdot n_t=200\cdot 200=40{,}000$$

PC scores for the first three components of PPM were plotted directly, and a trajectory through PC space was calculated by applying the coefficients to produce these components back to the raw perievent firing data.

An identical approach was taken for space, but here the grouping variable we used to combine vectors across sessions was the location of the rat associated with the instantaneous activity rather than the time of occurrence:

$$\vec{\text{PPV}}_{\text{space}}(X,Y,\text{iter})=\begin{bmatrix}\vec{\text{PV}}(1,\text{rand},X,Y)\\\vec{\text{PV}}(2,\text{rand},X,Y)\\\vdots\\\vec{\text{PV}}(\nu,\text{rand},X,Y)\end{bmatrix}$$

Rather than selecting randomly across trials, the spatial PVs are selected from the set of firing rates associated with a specific (X, Y) location in space. X and Y were bins that spanned the range of the recording apparatus, in 20 pixel (about 3 cm) square bins. After eliminating bins that were not visited by all of the rats in the experiment, 208 spatial bins remained, producing a spatial pseudopopulation matrix ($\underset{\text{space}}{\vec{PPV}}$) with a similar size as the one used in the temporal analysis:

$$M_{\text{space}}=n_{\text{iter}}\cdot n_{(X,Y)}=200\cdot 208=41{,}600$$

2.3.8 | Statistical analysis

No statistical tests were used to predetermine sample size, but the sample was similar or larger to those generally used within the field. Paired t tests were used to compare the slope and intercept from regressions of firing rate to running speed for each session, the firing rate at the trial start for correct and error trials, and pairwise correlation of PVs taken from within or across epochs. PV similarity for matched disparities of space were submitted to a one-way repeated measures analysis of variance (ANOVA; factors: epoch, distance). Significance testing for the GLM used to categorize neurons based on response type, and classifier used to identify epoch based on population activity are described above.

3 | RESULTS

We recorded the responses of hippocampal CA1 neurons while rats were engaged in a memory-guided odor discrimination task (Butterly et al., 2012). On each trial, a removable divider was lifted and rats ran from an intertrial waiting area to approach two cups containing scented digging medium (Figure 1a). Odors were drawn from a set of 16 distinct odors, presented in eight pairings with one odor in each pair always rewarded with a buried sucrose pellet. The odors and right or left position of the rewarded cup was randomized across trials. On some trials (Figure 1b,e), the rats happened to approach the rewarded cup first by chance, and dug for a reward. On other trials rats approached the unbaited cup first (Figure 1f), and either correctly refrained from digging (Figure 1c) or incorrectly dug for a reward (Figure 1d) after which the trial continued until they obtained the reward in the baited cup. Following the reward, rats returned to the intertrial waiting area. Recordings took place over a period of up to 10 days, as rats learned reward contingencies for two sequentially presented sets of odor pairings in a task design used to probe for mnemonic interference. Results of the investigation into interference have been reported previously (Bulkin et al., 2016).

3.1 | Individual neurons respond at trial boundaries

Many neurons showed transient increases in activity at the start and end of trials, often selective for one of these two epochs. Figure 1g,h shows the responses of example "trial start" and "trial end" neurons. The upper panels show responses that were strongly time-locked to the start and end of trials, despite considerable variability in timing of behavior (Figure 1e,f). The lower panels of Figure 1g,h show the trajectory of the rat with color indicating the IFR. These neurons frequently showed elevated activity across large areas but time locked to the trial start or end, suggesting that activity was better explained by the occurrence of the trial events rather than spatial factors.

The large numbers of neurons with activity patterns like those seen in Figure 1g,h led to transient increases in multiunit firing rate that began just before the start of trials (as the divider was lifted) and then again at the end of the trials as rats returned to the intertrial waiting area (Figure 2a–d). Similar to the example responses shown in Figure 1g,h, this activity was not purely attributable to spatial location since firing occurred at the start and end point along the full width of the box. Most neurons were selective for either the trial start or trial end (Figure 2e, blue and red), which may be partly attributable to the fact that rats traveled in different directions even though these epochs occurred in similar locations. However, these apparent "spatial" regions of elevated firing were clearly modulated by the start and end of trials. Firing measured at the same locations during epochs associated with the trial start and end was distinct (Figure 2g, red and blue traces), and was elevated compared to firing far from trial boundaries (Figure 2g, black trace), indicating that activity was not modulated solely by spatial location.

Transient activity at the start and end of the trials was not likely associated with sharp-wave ripples. Rats were rarely immobile at these times, and field potentials showed robust theta oscillations, and so ripples were probably infrequent at these times (Buzsáki, Horváth, Urioste, Hetke, & Wise, 1992). Increased activity at the trial start/end was also not solely attributable to increased running speed at the start and end of trials. Although activity was correlated with running speed overall, we found that firing rates were higher at the time of the trial start and trial end than at instances of similar running speed occurring during the trial and ITI epochs, indicating that trial start/end activity was higher than expected based on running speed alone (Supplemental Figure S1). To statistically confirm this, we computed a series of linear regressions for each session defining multiunit firing rate as a function of running speed, separately for data selected from the trial start and trial end and the ITI. The slopes of the resulting regression lines taken from the trial start/end data were similar to the slopes based on ITI data (paired t test, $p > .01$ for start and end), yet the intercept was significantly higher for data selected from the trial start (paired t test, $p < 10^{-6}$) and end (paired t test, $p < 10^{-6}$). A similar analysis showed that trial start/end responses were not due to acceleration (paired t test on intercepts; start: $p < 10^{-15}$ end: $p < 10^{-23}$, Supplementary Figure S1b). This suggests that activity at these times showed a global increase not attributable to running speed or acceleration.

Interestingly, the magnitude of the trial start response (average firing rate ±500 ms around trial start) was somewhat larger on trials in which the rat subsequently made a correct choice (Figure 2h; 641 units, paired t test: $p < .001$). This effect was probably not driven by reward related activity, or a reduction in the reward prediction error when rats identified the odor and could therefore predict an impending reward. Rats rarely arrived at the first cup within 500 ms (Figure 1e,f), and we saw no evidence of a decision (e.g., a change in trajectory) before this time.

To assess the relative contributions of spatial and temporal factors in shaping the activity of individual neurons, we modeled the firing rate of each neuron as a function of the rat's location and the time of the nearest trial start and trial end. Because position and time partially covaried (i.e., position was not random at times near the trial start and end), we used an extension of a constrained Poisson GLM that orthogonalizes covariates to disambiguate the independent contributions of factors affecting firing rate (Truccolo et al., 2004). This strategy has been previously used specifically for distinguishing effects in the face of nuisance correlations between factors shaping hippocampal activity (Lepage et al., 2012; MacDonald, Lepage, Eden, & Eichenbaum, 2011). For each neuron we fit three Gaussian functions to the average activity: two one-dimensional curves that described firing rate as a function of time with respect to trial start and end, and a two dimensional surface that described firing rate as a function of the location of the rat. We then described the firing rate of the neuron as the weighted sum of these three functions (effects of trial start, trial end, and position), using the projection described in Lepage et al. (2012) to form estimates of temporal effects that could not be accounted for by covariation between the times of trials and the location of the rat. Finally, we computed the statistical significance of each coefficient via a normal approximation of the

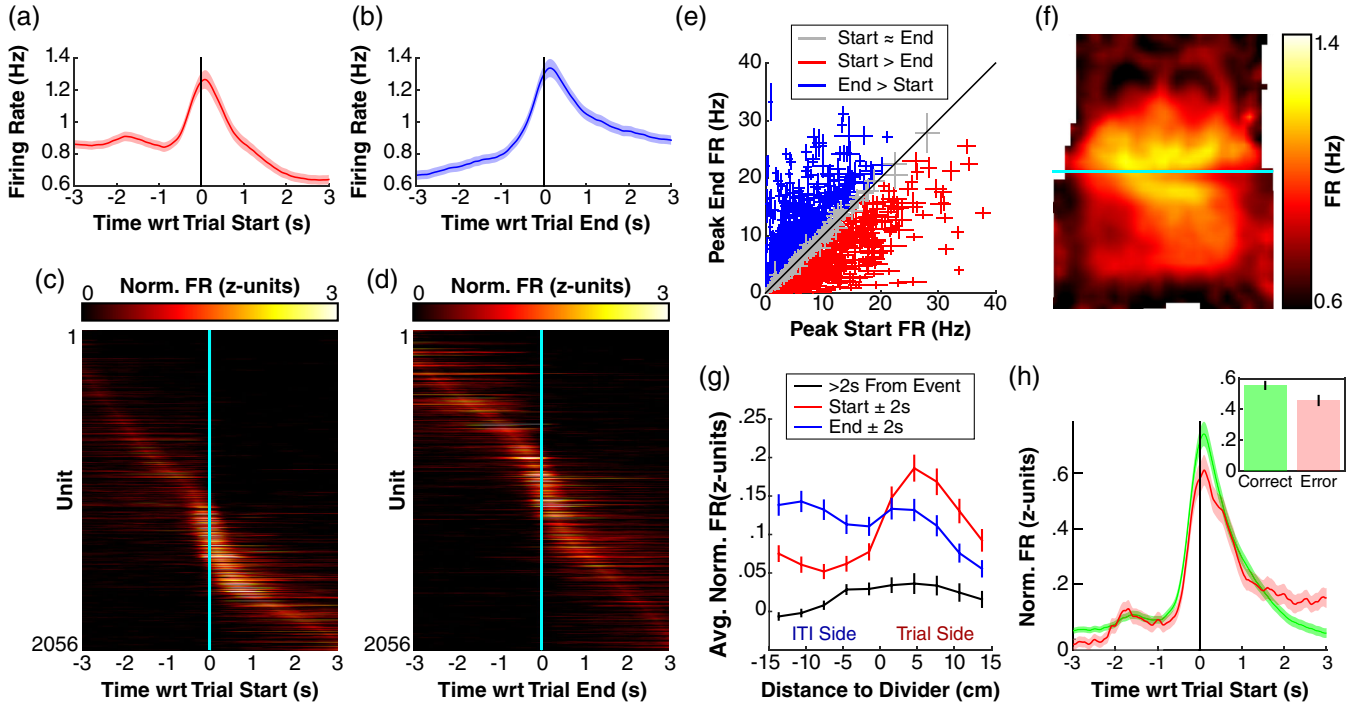

FIGURE 2 Increase in activity of hippocampal neurons at trial start and trial end. Panels (a) and (b) show average multiunit firing rate aligned on trial start and trial end. Firing rates of each unit were binned (100 ms bins) and smoothed with a five-bin moving average. The shaded region indicates *SEM* over units. Panels (c) and (d) show average normalized firing rate aligned on trial start and end for all units. Binned activity was normalized by *z*-scoring using the average and standard deviation of each unit's rate over the entire session. The trial-averaged traces were then sorted based on the time of the maximum rate. Panel (e) shows a scatterplot of peak firing rate of each neuron in a window ±3 s with respect to trial start (abscissa) versus trial end (ordinate). For each unit a single crosshair is plotted, centered on the average peak rate, and extending ±1 *SEM* (over trials). Units with *SEM* overlapping with unity are shown in gray (513/2,056 units), those above unity are shown in blue (810/2,056 units), and those that fall below unity are shown in red (733/2,056 units). Panel (f) shows the average firing rate in 1.5 cm^2 spatial bins. Points between the centers of the bins have been linearly interpolated. The horizontal line indicates the location of the removable divider (see Figure 1a). Panel (g) shows average multiunit firing rate for locations in 3 cm bins in the axis orthogonal to the divider (i.e., vertical in (f)), calculated separately for rates occurring within 2 s of the start of the trial (red) or end of the trial (blue) or more than 2 s from either (black). Panel (h) shows average firing rate around the start of the trial plotted separately for correct (green) and error (pink) trials, only neurons with trial start responses have been included (688 neurons, Figure 3a). The inset shows the average activity in a window ±500 ms on the trial start. Shaded region and error bars indicate *SEM* over units [Color figure can be viewed at wileyonlinelibrary.com]

bootstrap estimate (Efron & Tibshirani, 1994). Supplementary Figure S2a–f shows responses and fits of example temporally and spatially modulated neurons that were disambiguated by this analysis.

The majority of neurons were significantly modulated by space (1,601/2,056; Figure 3a). Yet, many of these neurons showed additional modulation by the trial start or end (859/1,601; Bonferroni corrected for tests of trial start and end responses). Importantly, because the model orthogonalized spatial and temporal covariates, the trial start/end responses were not spuriously identified due to rats traversing through a place field at the beginning or end of trials. Rather, neurons represented both location and time with respect to the trial boundaries. Approximately half of the neurons showed some modulation by one of the temporal factors (1,004/2,056, Bonferroni corrected), and similar numbers of cells had activity that was affected by the trial start and trial end (start: 688 neurons; end: 757 neurons). Plotting the average firing rate for start/end responsive and spatially sensitive neurons revealed that firing patterns were similar for neurons with a trial start/end response whether or not the neuron was also modulated by space, and that spatially sensitive neurons that lacked a trial start/end response showed larger firing rates during ITI epochs (Figure 3b,c; Supplemental Figure S2g,h). In order to control for the possible contribution of running speed to trial start/end firing, we repeated the GLM and included a linear term for running speed. Firing was modulated by running speed for many neurons (773/2,056), but accounting for variance due to running speed had little effect on the number of neurons marked as responsive to the trial start/end (Supplemental Figure S2i,j).

3.2 | Distinct population states represent the trial and ITI

Inspection of the neural activity in Figure 2 revealed two important details about the dynamics of hippocampal firing as rats started and ended trials: a prominent increase in firing at the trial boundaries (Figure 2a,b), and distinct populations of neurons were recruited during trial and ITI epochs (Figure 2c,d). Unlike the transient activity

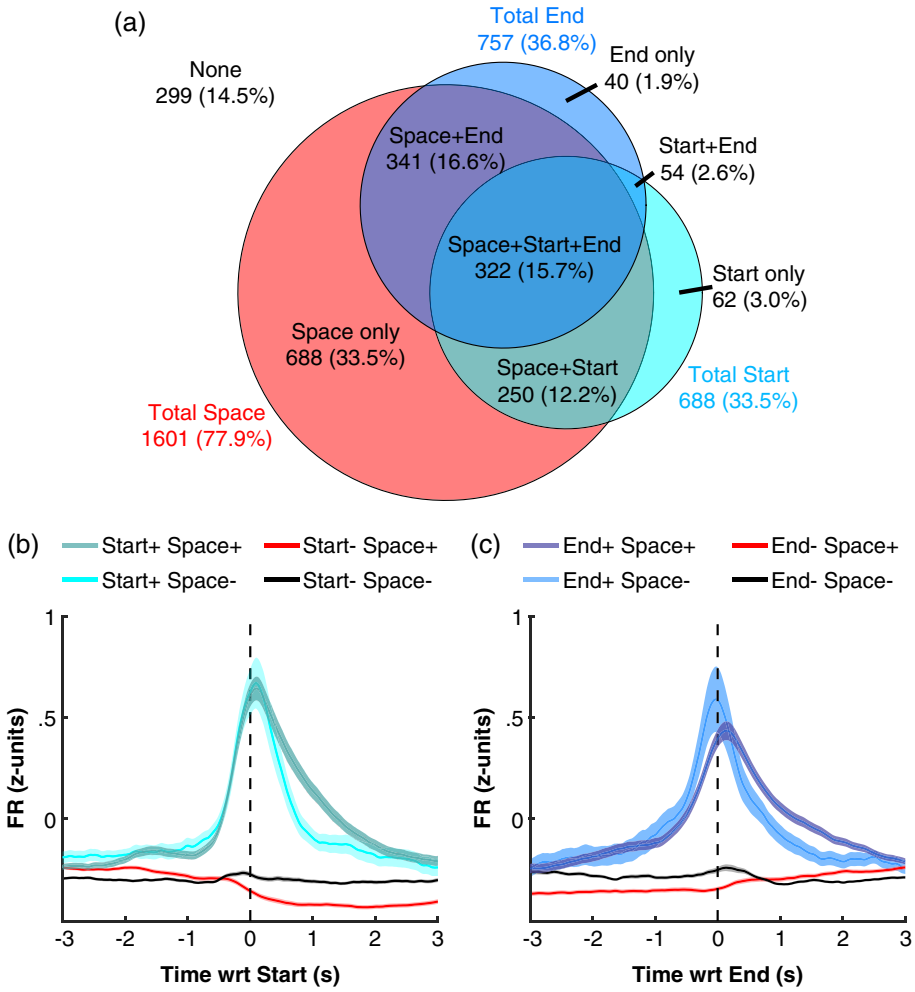

FIGURE 3 Independent spatial and temporal responses in overlapping neuronal populations. Panel (a) shows a Venn diagram indicating the classified responses of neurons. Each unit was submitted to a generalized linear model (GLM) which orthogonalized components defined by spatial and temporal Gaussian fits to average response data. The diagram tallies the number/percent of neurons with a significant term in the model for the noted component. Panels (b) and (c) show average normalized firing rate for units with (+) and without (–) significant spatial and trial start (b) or trial end (c) coefficients. The GLM successfully identified start and end responsive neurons, evidenced by the clear peak in the average firing rate of these neurons compared with unresponsive neurons. Units classified as exclusively spatial (i.e., start–/end–/space+) showed somewhat elevated firing rates in the intertrial interval (ITI; before the trial start in (b) and after the trial end in (c)) [Color figure can be viewed at wileyonlinelibrary.com]

increases at the trial boundaries, nonoverlapping populations during trials and ITIs are potentially consistent with spatial models of hippocampal activity as these two epochs were necessarily in distinct spatial locations (Figure 1a). We next performed a series of population analyses to understand whether differences in firing patterns during the trial and ITI could be explained simply by differences in the rat's position, or whether trial boundaries marked a state transition such that differences in firing patterns exceeded what would be expected based on positional disparity alone.

To measure ensemble similarity, we tabulated PVs (vectors containing firing rates in 100 ms bins) and computed pairwise correlations between them. We averaged the pairwise correlation coefficients between PVs drawn from different trials, at times surrounding the start and end of trials (±3 s). Figure 4a,b shows the average values (across recording sessions) for each pair of comparisons. The color of each point in the images indicates the average cross-trial correlation between one temporal bin and another. Points lying on unity quantify the similarity of ensemble activity from trial to trial at the same time with respect to the trial start/end, while off-unity points indicate cross-trial similarity at proximal times.

Examination of the cross-trial correlation plots (Figure 4a,b) reveals several striking characteristics of large scale hippocampal activity patterns. Both plots show a strong peak at the center, indicating that trial start/end firing patterns are similar from one trial to the next, an outcome which reflects the reliable bursts of firing seen at the trial boundaries (Figure 2a,b). Correlations along the unity line declined from this peak as time passed from the trial start, but remained high throughout the trial epoch. For example, firing patterns occurring ~1.5 s into the trials (see ●, Figure 4a) were surprisingly well correlated across trials. At that time, the rats had typically arrived at the first odor cup (Figure 1e,f), encountered one of the 16 possible odor cues, and decided whether to dig or proceed to the second cup, depending on the valence of the odor cue. Even more noteworthy, firing patterns taken from quite distant times within the trials were also well correlated. For example, the firing patterns occurring 0.5 s into the trial were surprisingly similar to firing occurring 2 s later (i.e., 2.5 s into the trial, see ♦, Figure 4a), despite the fact that the rats were engaged in markedly different and highly variable behaviors at those two time points (Figure 1e,f). Rats were nearly always approaching the first odor cup at 0.5 s, but at the 2.5 s time point they could be digging in the first cup, investigating or digging in the second cup (if the first cup was not rewarded), consuming the reward, or returning to the ITI side of the chamber. This was not likely driven by spatial location since the trial structure meant that rats rarely occupied the

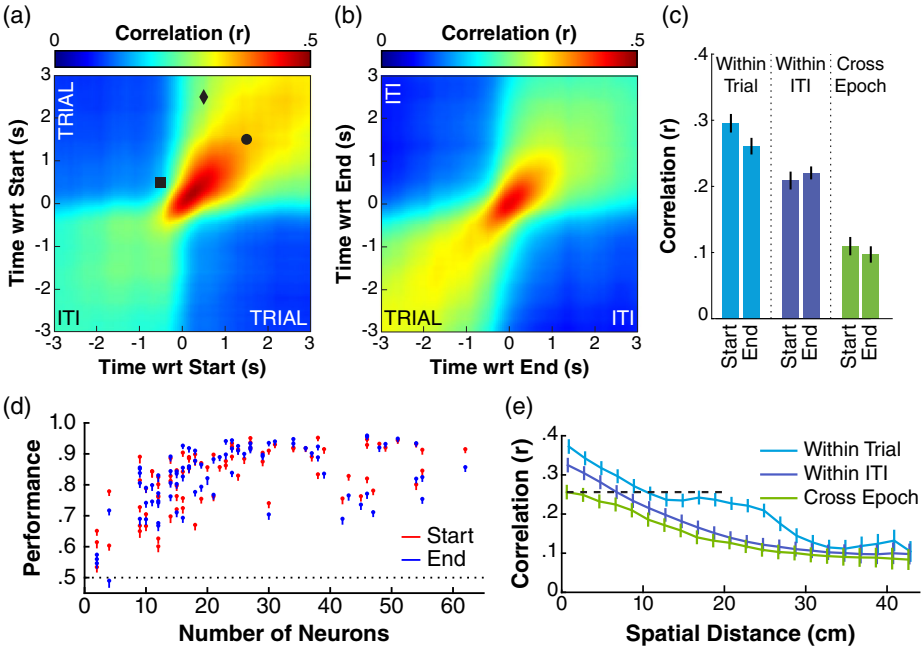

FIGURE 4 Distinct population states during trials and intertrial intervals (ITIs). Panels (a) and (b) show cross-trial PV correlations around trial start and trial end. For each session, firing rates were tabulated to form PVs and pairwise correlations were computed using vectors in a 6 s window around the trial start (a) or end (b) from different trials (each pairwise correlation involved two unique trials at two time points). Correlation values were averaged to form a map for each recording session; the average of these maps is shown. Points in the image between bins have been linearly interpolated. The symbols overlaid on the plot in (a) highlight times of interest discussed in the text. Panel (c) shows a summary of cross-trial correlations. The height of the bars indicates the average value in the corresponding quadrant of the maps shown in (a,b). Error bars indicate *SEM* across sessions. Panel (d) measures the performance of a linear discriminant classifier trained with a subset (50%) of PVs selected from trials and ITIs to classify the epoch of the vector (i.e., whether it occurred in an ITI or a trial). The classifier was tested separately on vectors selected from a window 3 s before/after the trial start (red points) and trial end (blue points). Confidence intervals were estimated using an iterative process, randomly selecting vectors 1,000 times, with the 5% lower confidence interval identified as the fifth percentile of the iterated dataset. Lines span from this point to the median performance across iterations for each session. The abscissa indicates the number of simultaneously recorded neurons in the session. Panel (e) shows pairwise correlations between population vectors as a function of the distance between positions that the rat occupied when the activity occurred. Correlations were computed separately for pairs in which both vectors were selected from trial epochs (cyan), ITI epochs (blue), or when one vector was selected from each epoch (green). The dashed line highlights a comparison discussed in the text. Error bars indicate *SEM* [Color figure can be viewed at wileyonlinelibrary.com]

same location at these two different time points (Figure 1b–d). Firing patterns within the ITI epoch also showed a large degree of similarity (Figure 4a,b, lower left and upper right, respectively), although these correlations were significantly lower than those for PVs taken from the trial epoch (Figure 4c; paired *t* test: $T(83) = 4.59$, $p < 10^{-4}$).

Another important feature that is apparent in these plots is the sharp boundary between the trial and ITI epochs. In contrast to the remarkable self-similarity of firing patterns taken from within an epoch, correlations were significantly lower for vectors drawn from different epochs (Figure 4c; paired *t* tests: ITI vs. cross $T(83) = 18.89$, $p < 10^{-31}$; trial vs. cross $T(83) = 14.27$, $p < 10^{-23}$). This suggests that activity was distinct across the two epochs (Figure 4a,b, upper left and lower right). Indeed, correlations for vectors taken only 1 s apart but from different epochs (i.e., 0.5 s before and 0.5 s after trial start, see ■, Figure 4a) were much lower than those for vectors taken twice as far apart but within the trial epoch (see ♦, Figure 4a). Similar patterns were found when correlations were measured using Kendall's rank correlation coefficient, which is arguably more robust to the relatively sparse firing patterns seen in hippocampus (Neymotin, Talbot, Jung, Fenton, & Lytton, 2017) (Supplementary Figure S3a–c).

The striking self-similarity of firing patterns within each epoch, and the sharp decline in similarity when rats transitioned from the trial epoch to the ITI, suggest that hippocampus treats these two epochs as distinct contexts. Consistent with this idea, we could accurately decode population activity as belonging to the trial or ITI using linear discriminant analysis. We used an iterative process wherein we trained linear classifiers using a randomly selected subset of half of the PVs and measured performance of the classifiers on the remaining half. We repeated this process 1,000 times, providing a distribution of performance values (proportion of PVs correctly classified). Classifier performance (Figure 4d) was virtually always above chance, and showed high accuracy: on average 85% of vectors surrounding the trial start and 84% of vectors surrounding the trial end were correctly classified. Classification errors were most likely to occur near the trial boundaries (Supplementary Figure S3f,g), a period when ensembles encoded the boundary itself rather than the surrounding epoch.

While hippocampal output reliably differentiated the task epochs, the increased similarity of ensemble activity within epochs could simply be due to spatial factors since any two PVs drawn from a single epoch were more likely to correspond nearby locations than two PVs selected from different epochs. Even the greater similarity within trials than within the ITI could have been influenced by spatial factors since spatial behavior was more constrained during trials. In order to determine whether these spatial factors did, in fact, account for the within-epoch similarity, we compared PV correlations for subsets of data with fixed ranges of spatial distance. We labeled each pair of PVs using the distance between the associated positions (locations occupied by the rat at the time of the PV) and binned pairwise correlation values based on distances (Figure 4e). If ensemble activity was governed purely by space, the selected epoch would make no difference in the correlation values and an overall decrease in correlation with distance would be expected. In fact, even at very low distances, PVs were more similar within epochs than across epochs, and within trial similarity was higher than within ITI similarity (repeated measures ANOVA: main effect of epoch $F(2,166) = 19.15$, $p < 10^{-7}$; main effect of distance $F(21,1743) = 182.9$, $p < 10^{-15}$; interaction $F(42,3486) = 6.053$, $p < 10^{-15}$). Indeed, correlations for PVs taken 10–20 cm apart during a trial were as similar as PVs taken just 1 cm apart but which spanned the trial start boundary (Figure 4e, dashed line). This increased similarity between vectors selected from trial epochs persisted at larger distances, with a noticeable "bump" in the similarity curve for PVs that occurred when positions were separated by about 20 cm. This distance is of particular note as the odor stimuli used in the experiment were presented in cups separated by 20 cm (Figure 1a) and we occasionally observed examples of individual neurons that showed increased activity as rats sampled the odors and dug in the cups, regardless of which cup (see also Eichenbaum, Kuperstein, Fagan, and Nagode (1987) and Muzzio et al. (2009)). The observation that the trial and ITI epochs were more similar than would be suggested by spatial considerations alone is consistent with the idea that the hippocampus represents the two epochs as distinct contexts and differentiates them accordingly.

3.3 | Dynamics of hippocampal ensembles during state transitions

The dissimilarity between population activity in trial and ITI epochs, above what is predicted from space alone, suggests that hippocampal ensembles undergo a comprehensive state transition at the start and end of each trial. Analogous to the role of heat in phase transitions, the increase in hippocampal multiunit activity at the start and end of trials might serve to drive this transition, pushing the hippocampal state past a critical point to allow a shift in representational state (Steyn-Ross, Steyn-Ross, Wilson, & Sleigh, 2010). As such, we next sought to characterize the hippocampal state itself rather than relying on pairwise correlations to make inferences about the clustering of hippocampal representations. We took a dimension reduction strategy using principal component analysis (PCA). Because PCA produces an orthogonal transformation to a set of linearly uncorrelated variables accounting for descending quantities of variance, it allows for a representation of high dimensional neural activity that captures important covariation among ensembles. However, while the individual components identify a mapping of the raw data based on variance, the sign of PC scores is irrelevant. Thus, averaging PC scores across sessions provides no information on how a typical ensemble changes. To circumvent this issue, we built a large matrix of pseudo-PVs containing the firing rates of all of the units in our dataset ($n = 2056$). To combine PVs across multiple sessions, we labeled vectors based on their time relative to the trial start and trial end. We took activity from 100 ms bins extending ±5 s around each trial's start and end. We then randomly sampled (with replacement) a vector from a given bin from each session 200 times, generating typical 2,056 dimensional vectors for that moment in time. Repeating this process across bins produced a matrix with 40,000 observations (200 time points × 200 iterations). We subjected this entire matrix to PCA. Importantly, although the pseudo-PV matrix was assembled using temporal labels, PCA is blind to these labels and simply provides loadings (i.e., a coefficient for each neuron) such that the first principal component accounts for maximal variance and each additional component accounts for a decreasing amount of variance.

Figure 5a shows a three-dimensional plot of the scores of the first three principal components for each vector in the pseudo-PV. Points taken from the ITI (before trial start or after trial end) are shown in cooler colors, and points during trials (after trial start or before trial end) are shown in warmer colors. A curve showing the trajectory through PC space was constructed by applying the coefficients identified from PCA back to the (raw) average firing rates in the time ±5 s around the trial start and end. The projections of this three-dimensional representation to each of the two-dimensional planes are shown as "shadows" on the axes. PC1, capturing the largest amount of variance, distinguished the epochs: trials and ITIs formed completely nonoverlapping clusters (Figure 5b; see blue vs. red clusters in Figure 5a). PC2 identified trial boundaries, clearly distinct from the trial and ITI epochs, but not from each other (Figure 5c). PC3 made this distinction, differentiating trial start activity from trial end activity (Figure 5d). These results provide a view of the state transition of hippocampal ensembles over the course of trials. Despite a variety of individual neural firing patterns in the trial and ITI epochs, clear clusters of ensemble activity form that identify these distinct contexts. At the start and end of trials, ensembles transition from one representation to the other by traversing orthogonally through the trial start and trial end PC space.

To confirm that this approach yielded a view of the hippocampal state that was not artificially imposed by grouping vectors based on time with respect to trial boundaries, we repeated the analysis but combined vectors across sessions using a purely spatial method. To do this, we formed a matrix of PVs for each session, and labeled each vector with the position of the rat at the time associated with the activity. We then sampled PVs from each session (with replacement), concatenating vectors that occurred when the rat was in the same spatial bin (3 cm^2 bins). In this manner, we formed a large matrix of vectors in 2,056 dimensional spaces, each vector marking typical population firing rates for a particular spatial location. This is an identical

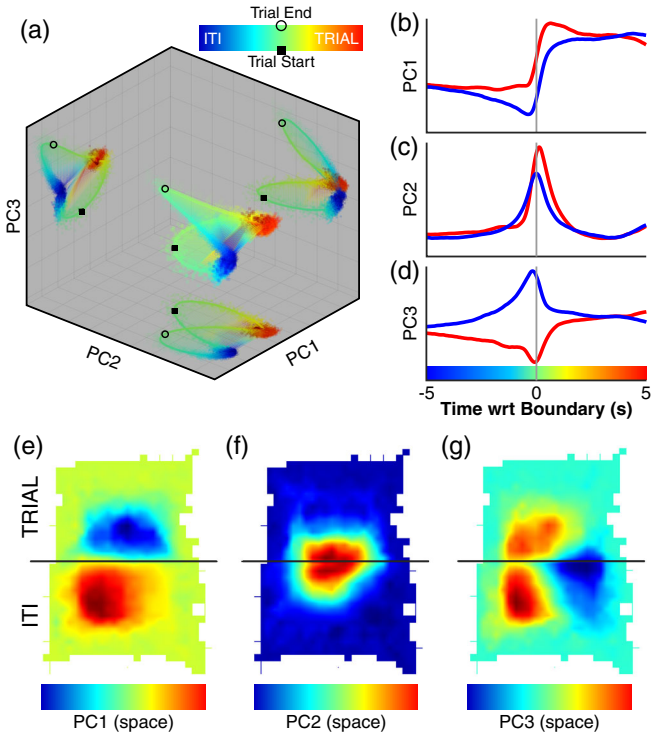

FIGURE 5 Principal component analysis (PCA) indicates a phase transition at trial start and end. Using a bootstrap approach, a pseudopopulation vector (PV) matrix was assembled to simulate typical firing vectors at time points ±5 s around the trial start and end. This matrix was submitted to PCA to obtain principal component scores for each time sample. (a) Three-dimensional plot of the first three principal component scores (brightly colored illustration in the center). Two-dimensional shadow projections of the three-dimensional data are shown on the walls (the three darker images), illustrating the degree to which each pair of principal components segregates the trial epochs. Colored dots indicate scores of the principal components around the trial start and trial end, with warmer colors indicating times in the trial while cooler colors indicate times in the ITI. The start and end are indicated with black markers (square and circle respectively). A line traces the trajectory through PC space, computed by applying the coefficients obtained by PCA and taking the weighted mean of average perievent firing (Figure 1c,d). The colored surface is shown to aid interpretation of the three-dimensional structure, and was formed by linear interpolation. (b–d) The PC data shown in (a), plotted as a function of time for each principal component. As with the line shown in (a), these values were computed by applying the coefficients obtained from PCA to the average firing rate traces for each unit. (e–g) Spatial PC heatmaps computed using the same strategy as in Panel (a), but assembling a pseudopopulation matrix based on spatial location rather than the time of individual PVs (see text). Coefficients from PCA were applied to the individual unit spatial firing heatmaps to compute a weighted average. The maps have been linearly interpolated between sampled locations [Color figure can be viewed at wileyonlinelibrary.com]

procedure to the method described above but here vectors were combined based on spatial location of the rat rather than the time with respect to trial start and end. We subjected the spatial pseudo-PV to PCA to obtain coefficients for each neuron, and used the coefficients to create average spatial maps in PC space (Figure 5e–g). The pattern is strikingly similar to what we found with our time locked analysis. PC1 distinguished the trial and ITI epochs, it was most distinct between regions associated with trials and ITIs (compare Figure 5e top and bottom). PC2 marked the trial boundaries, values near the divider are distinct from values far from the divider (Figure 5f). In contrast to the time locked analysis where PC3 distinguished the trial start and end (Figure 5d), the spatially binned PCA did not clearly distinguish them (Figure 5g), possibly because the trial start and end occurred in overlapping spatial locations.

The strong hippocampal transitions at trial boundaries were specifically dependent on trial start/end responsive neurons. When the same analysis was restricted to the subset of neurons with significant trial start or end responses as identified with our GLM approach (Figure 3), the shape of the resulting pattern in PC space was virtually identical (Supplementary Figure S4a). Yet, the pattern was completely different when the neurons without trial start/end responses were analyzed (Supplementary Figure S4b), despite the similarity in sample size (1,004 responsive vs. 1,052 unresponsive cells). The separation between ITI and trial PVs captured by PC1 was preserved when trial start/end cells were excluded, but the transitional signals between trials and ITIs that were evident in PC2 and PC3 were completely eliminated.

4 | DISCUSSION

In this article, we examined the responses of many hippocampal neurons while rats engaged in an olfactory memory task with a repeated trial structure. We focused our analyses on activity differences between trials and ITIs, as well as the transition between these epochs. We observed a large-scale shift in the activity state of the hippocampus at the start and end of trials, a transient increase in activity that marked a transition between two highly distinct states. We found that individual neurons were modulated by both spatial and temporal factors, driving an ensemble representation that clearly identified the trial and ITI epochs and the boundaries between them, the trial start and trial end. The dynamics resembled a phase-transition-like pattern: populations transformed from one steady state to another at the moment of trial start or end, with a transient increase in firing that occurred at the transitions.

The self-similarity of hippocampal firing patterns from one trial to another was striking. Although different trials shared some behavioral and sensory features (removal and insertion of the divider, running speed patterns, investigation of odors, digging for and consumption of the reward), there was also a substantial variation from one trial to the next. Differences included the trajectory of the rat, the olfactory experience of 16 distinct odors, the position of the reward, and whether the rewarded odor was encountered first by chance or the initial odor cup was rejected in favor of the second. Notably, we observed highly similar firing patterns across trials despite these highly distinct patterns of sensory input and motor behavior. Because the sequence of events in the trials was determined by the voluntary behavior of the rat and randomization procedures (e.g., left or right

location of the rewarded odor cup), the rat's experience became increasingly distinct as the trial progressed. Neural activity also decreased in similarity over the course of a trial, but remained surprisingly well correlated. This is especially striking for correlations of time points that were several seconds apart, when location, behavior, and sensory experience were virtually always different (Figure 4a). Notably, these observations also suggest that differences in firing patterns between the trial and ITI are probably not attributable to behavioral differences between the two epochs. If large differences in behavior did not cause differential firing within the trial epoch, it is unlikely that such behavioral differences could explain differential firing patterns across epochs. Overall, these results are consistent with previous findings that hippocampal firing patterns occupy a local minimum in state space where firing patterns are relatively stable and insensitive to small changes in the environment, until environmental change is sufficient to abruptly push the firing patterns into a new state space (Wills et al., 2005). However, previous studies involved subtle changes in the shape of the environment and similar foraging behaviors. Here, we show that a self-similar hippocampal state persists even in the face of highly variable sensory input and behaviors during the performance of a complex memory task.

The observation of an abrupt shift in the representation when the rats transitioned between the trials and ITIs is similar to findings from studies that manipulated the environmental context (Jezek et al., 2011; Kelemen & Fenton, 2010; Wills et al., 2005), suggesting that the hippocampus treated the trial and ITI areas as distinct contexts even though they were both part of a familiar contiguous environment which was only divided by a barrier for part of the time. Consistent with this idea, firing patterns in the ITI and trial were more distinct than would be expected based on spatial distance alone, even for immediately adjacent locations (Figure 3e). This may be due to the markedly different cognitive-behavioral demands and motivational characteristics of the trial and ITI epochs since changes in the behavioral context are also known to induce remapping (Eschenko & Mizumori, 2007; Griffin, Eichenbaum, & Hasselmo, 2007; Kennedy & Shapiro, 2009; Skaggs & McNaughton, 1998; Smith & Mizumori, 2006). Indeed, Kelemen and Fenton (2010) showed that even in a single environment, the hippocampus can maintain two distinct maps and rapidly shift between them as needed to meet dynamic behavioral demands. Our findings are consistent with the idea that the hippocampus encodes contextual information, broadly defined to include spatial and nonspatial features of the situation (Smith & Bulkin, 2014).

The large multiunit firing bursts we observed at the trial start and trial end were not simply an artifact of increased running speed. However, we cannot rule out the possibility that the bursts may have been driven by a complex combination of sensory and motor factors including a sudden increase in speed in a particular direction or toward a particular goal cup, which coincides with a large change in the visual scene due to the removal of the divider. Cognitive factors such as expectations about the upcoming events of the trial may also play a role and interact with these sensory-motor variables (e.g., Skaggs & McNaughton, 1998). Regardless of the specific causal factors, the fact that the multiunit bursts coincided with the transition between two distinct hippocampal representations raises the possibility that the bursts might serve to drive firing patterns out of one attractor space and into another (Rolls, 2007; Wills et al., 2005), by pushing activity past a critical point to allow a shift in representational state (Steyn-Ross et al., 2010; Tkačik et al., 2015). Previous studies have identified neuronal responses near the start or end of trials (Ainge, Tamosiunaite, Woergoetter, & Dudchenko, 2007; Grieves, Wood, & Dudchenko, 2016; Hollup, Molden, Donnett, Moser, & Moser, 2001; Smith & Mizumori, 2006), but the potential impact of these responses on population dynamics was only apparent when we examined the activity of large numbers of neurons.

Another intriguing, if speculative, possibility is that trial start and end bursts may be involved in demarcating event boundaries. A growing literature has implicated the human hippocampus in the process of event segmentation (Baldassano et al., 2017; Ben-Yakov & Dudai, 2011; Ben-Yakov, Eshel, & Dudai, 2013; Ben-Yakov & Henson, 2018; Ben-Yakov, Rubinson, & Dudai, 2014; DuBrow & Davachi, 2013; Milivojevic, Varadinov, Vicente Grabovetsky, Collin, & Doeller, 2016), the process of breaking continuous experience into discrete episodes (Zacks & Swallow, 2007). Hippocampal involvement in encoding the sequence of events (Agster, Fortin, & Eichenbaum, 2002; Davachi & DuBrow, 2015; Fortin, Agster, & Eichenbaum, 2002; Hasselmo & Eichenbaum, 2005) is consistent with an event segmentation account. The boundaries of behaviorally defined events often coincide with spatial boundaries, and neurons in the hippocampus and related structures are sensitive to physical barriers (Hinman, Chapman, & Hasselmo, 2019; Lever, Wills, Cacucci, Burgess, & O'Keefe, 2002; Solstad, Boccara, Kropff, Moser, & Moser, 2008) and other important spatial boundaries such as entering a room or a new street (Javadi et al., 2017; Spiers, Hayman, Jovalekic, Marozzi, & Jeffery, 2015). Indeed, event boundaries are often defined by a change in context, such as moving from one room to another or changing from one behavioral task to another (Horner, Bisby, Wang, Bogus, & Burgess, 2016), as in the present study. Our results contain some fascinating similarities to human studies of event segmentation. The trial start/end responses we observed are consistent with BOLD increases seen at event boundaries in human subjects (Baldassano et al., 2017; Ben-Yakov & Henson, 2018) and our finding that a stronger response to the trial start was associated with better performance is consistent with the well-documented link between event segmentation and memory performance in humans (Sargent et al., 2013; Zacks, Speer, Vettel, & Jacoby, 2006). However, we emphasize that our task was not designed to investigate event segmentation, but was instead designed to study the hippocampal role in mitigating proactive interference (Bulkin et al., 2016). The highly predictable and repeating trial structure of our task is quite different from studies of spontaneous event segmentation in humans (Sargent et al., 2013; Zacks et al., 2006), and we cannot distinguish between representational changes caused by the beginning of a new event from representational shifts caused by behavioral and environmental factors that cooccurred with the trial boundaries, such as the sensory-motor factors mentioned above and the expectation of a discrimination test and reward. Whether the rodent hippocampus, like the human hippocampus, is active at event

boundaries that are not associated with large behavioral and environmental changes remains an important open question.

ACKNOWLEDGMENTS

The authors thank Leela Patel, Carly Britton, and Luke Grosvenor for their assistance with animal training and electrode hyperdrive fabrication. The authors also would like to thank Khena Swallow and Sam Whitehead for their feedback on the analyses and development of ideas presented in the manuscript. This work was supported by the National Institute of Mental Health (R01 MH083809 to D.M.S.).

DATA AVAILABILITY STATEMENT

The data that support the findings of this study are available from the corresponding author upon reasonable request.

ORCID

David M. Smith https://orcid.org/0000-0002-5156-8099

REFERENCES

Agster, K. L., Fortin, N. J., & Eichenbaum, H. (2002). The hippocampus and disambiguation of overlapping sequences. *The Journal of Neuroscience*, *22*, 5760–5768.

Ainge, J. A., Tamosiunaite, M., Woergoetter, F., & Dudchenko, P. A. (2007). Hippocampal CA1 place cells encode intended destination on a maze with multiple choice points. *The Journal of Neuroscience*, *27*, 9769–9779.

Alme, C. B., Miao, C., Jezek, K., Treves, A., Moser, E. I., & Moser, M.-B. (2014). Place cells in the hippocampus: Eleven maps for eleven rooms. *Proceedings of the National Academy of Sciences of the United States of America*, *111*, 18428–18435.

Anderson, M. I., & Jeffery, K. J. (2003). Heterogeneous modulation of place cell firing by changes in context. *The Journal of Neuroscience*, *23*, 8827–8835.

Baldassano, C., Chen, J., Zadbood, A., Pillow, J. W., Hasson, U., & Norman, K. A. (2017). Discovering event structure in continuous narrative perception and memory. *Neuron*, *95*, 709–721.e5.

Ben-Yakov, A., & Dudai, Y. (2011). Constructing realistic engrams: Poststimulus activity of hippocampus and dorsal striatum predicts subsequent episodic memory. *The Journal of Neuroscience*, *31*, 9032–9042.

Ben-Yakov, A., Eshel, N., & Dudai, Y. (2013). Hippocampal immediate poststimulus activity in the encoding of consecutive naturalistic episodes. *Journal of Experimental Psychology. General*, *142*, 1255–1263.

Ben-Yakov, A., & Henson, R. (2018). The hippocampal film-editor: Sensitivity and specificity to event boundaries in continuous experience. *The Journal of Neuroscience*, *38*(47), 518–524.

Ben-Yakov, A., Rubinson, M., & Dudai, Y. (2014). Shifting gears in hippocampus: Temporal dissociation between familiarity and novelty signatures in a single event. *The Journal of Neuroscience*, *34*, 12973–12981.

Bulkin, D. A., Law, L. M., & Smith, D. M. (2016). Placing memories in context: Hippocampal representations promote retrieval of appropriate memories. *Hippocampus*, *26*, 958–971.

Butterly, D. A., Petroccione, M. A., & Smith, D. M. (2012). Hippocampal context processing is critical for interference free recall of odor memories in rats. *Hippocampus*, *22*, 906–913.

Buzsáki, G., Horváth, Z., Urioste, R., Hetke, J., & Wise, K. (1992). High-frequency network oscillation in the hippocampus. *Science*, *256*, 1025–1027.

Colgin, L. L., Moser, E. I., & Moser, M. B. (2008). Understanding memory through hippocampal remapping. *Trends in Neurosciences*, *31*, 469–477.

Davachi, L., & DuBrow, S. (2015). How the hippocampus preserves order: The role of prediction and context. *Trends in Cognitive Sciences*, *19*, 92–99.

DuBrow, S., & Davachi, L. (2013). The influence of context boundaries on memory for the sequential order of events. *Journal of Experimental Psychology. General*, *142*, 1277–1286.

Efron, B., & Tibshirani, R. (1994). *An introduction to the bootstrap*. Chapman & Hall, United Kingdom.

Eichenbaum, H., Kuperstein, M., Fagan, A., & Nagode, J. (1987). Cue-sampling and goal-approach correlates of hippocampal unit activity in rats performing an odor-discrimination task. *The Journal of Neuroscience*, *7*, 716–732.

Eschenko, O., & Mizumori, S. J. Y. (2007). Memory influences on hippocampal and striatal neural codes: Effects of a shift between task rules. *Neurobiology of Learning and Memory*, *87*, 495–509.

Ferbinteanu, J., & Shapiro, M. L. (2003). Prospective and retrospective memory coding in the hippocampus. *Neuron*, *40*, 1227–1239.

Fortin, N. J., Agster, K. L., & Eichenbaum, H. B. (2002). Critical role of the hippocampus in memory for sequences of events. *Nature Neuroscience*, *5*, 458–462.

Gonçalves, S., & Politis, D. (2011). Discussion: Bootstrap methods for dependent data: A review. *Journal of the Korean Statistical Society*, *40*, 383–386.

Grieves, R. M., Wood, E. R., & Dudchenko, P. A. (2016). Place cells on a maze encode routes rather than destinations. *eLife*, *5*, e15986.

Griffin, A. L., Eichenbaum, H., & Hasselmo, M. E. (2007). Spatial representations of hippocampal CA1 neurons are modulated by behavioral context in a hippocampus-dependent memory task. *The Journal of Neuroscience*, *27*, 2416–2423.

Hasselmo, M. E., & Eichenbaum, H. (2005). Hippocampal mechanisms for the context-dependent retrieval of episodes. *Neural Networks*, *18*, 1172–1190.

Hinman, J. R., Chapman, G. W., & Hasselmo, M. E. (2019). Neuronal representation of environmental boundaries in egocentric coordinates. *Nature Communications*, *10*, 2772.

Holland, P. C., & Bouton, M. E. (1999). Hippocampus and context in classical conditioning. *Current Opinion in Neurobiology*, *9*, 195–202.

Hollup, S. A., Molden, S., Donnett, J. G., Moser, M. B., & Moser, E. I. (2001). Accumulation of hippocampal place fields at the goal location in an annular watermaze task. *The Journal of Neuroscience*, *21*, 1635–1644.

Horner, A. J., Bisby, J. A., Wang, A., Bogus, K., & Burgess, N. (2016). The role of spatial boundaries in shaping long-term event representations. *Cognition*, *154*, 151–164.

Javadi, A.-H., Emo, B., Howard, L. R., Zisch, F. E., Yu, Y., Knight, R., … Spiers, H. J. (2017). Hippocampal and prefrontal processing of network topology to simulate the future. *Nature Communications*, *8*, 14652.

Jezek, K., Henriksen, E. J., Treves, A., Moser, E. I., & Moser, M. B. (2011). Theta-paced flickering between place-cell maps in the hippocampus. *Nature*, *478*, 246–249.

Kelemen, E., & Fenton, A. A. (2010). Dynamic grouping of hippocampal neural activity during cognitive control of two spatial frames. *PLoS Biology*, *8*, e1000403.

Kennedy, P. J., & Shapiro, M. L. (2009). Motivational states activate distinct hippocampal representations to guide goal-directed behaviors. *Proceedings of the National Academy of Sciences of the United States of America*, *106*, 10805–10810.

Law, L. M., & Smith, D. M. (2012). The anterior thalamus is critical for overcoming interference in a context-dependent odor discrimination task. *Behavioral Neuroscience*, *126*, 710–719.

Lepage, K. Q., MacDonald, C. J., Eichenbaum, H., & Eden, U. T. (2012). The statistical analysis of partially confounded covariates important to neural spiking. *Journal of Neuroscience Methods*, *205*, 295–304.

Leutgeb, J. K., Leutgeb, S., Moser, M.-B., & Moser, E. I. (2007). Pattern separation in the dentate gyrus and CA3 of the hippocampus. *Science*, *315*, 961–966.

Leutgeb, S., Leutgeb, J. K., Barnes, C. A., Moser, E. I., McNaughton, B. L., & Moser, M. B. (2005). Independent codes for spatial and episodic memory in hippocampal neuronal ensembles. *Science*, *309*, 619–623.

Lever, C., Wills, T., Cacucci, F., Burgess, N., & O'Keefe, J. (2002). Long-term plasticity in hippocampal place-cell representation of environmental geometry. *Nature*, *416*, 90–94.

MacDonald, C. J., Lepage, K. Q., Eden, U. T., & Eichenbaum, H. (2011). Hippocampal "time cells" bridge the gap in memory for discontiguous events. *Neuron*, *71*, 737–749.

Milivojevic, B., Varadinov, M., Vicente Grabovetsky, A., Collin, S. H. P., & Doeller, C. F. (2016). Coding of event nodes and narrative context in the hippocampus. *The Journal of Neuroscience*, *36*, 12412–12424.

Muller, R. U., & Kubie, J. L. (1987). The effects of changes in the environment on the spatial firing of hippocampal complex-spike cells. *The Journal of Neuroscience*, *7*, 1951–1968.

Muzzio, I. A., Levita, L., Kulkarni, J., Monaco, J., Kentros, C., Stead, M., … Kandel, E. R. (2009). Attention enhances the retrieval and stability of visuospatial and olfactory representations in the dorsal hippocampus. *PLoS Biology*, *7*, e1000140.

Nadel, L. (2008). The hippocampus and context revisited. In S. J. Mizumori (Ed.), *Hippocampal place fields: Relevance to learning and memory* (pp. 3–15). New York, NY: Oxford University Press.

Neymotin, S. A., Talbot, Z. N., Jung, J. Q., Fenton, A. A., & Lytton, W. W. (2017). Tracking recurrence of correlation structure in neuronal recordings. *Journal of Neuroscience Methods*, *275*, 1–9.

Peters, G. J., David, C. N., Marcus, M. D., & Smith, D. M. (2013). The medial prefrontal cortex is critical for memory retrieval and resolving interference. *Learning & Memory*, *20*, 201–209.

Rolls, E. T. (2007). An attractor network in the hippocampus: Theory and neurophysiology. *Learning & Memory*, *14*, 714–731.

Rudy, J. W. (2009). Context representations, context functions, and the parahippocampal-hippocampal system. *Learning & Memory*, *16*, 573–585.

Sargent, J. Q., Zacks, J. M., Hambrick, D. Z., Zacks, R. T., Kurby, C. A., Bailey, H. R., … Beck, T. M. (2013). Event segmentation ability uniquely predicts event memory. *Cognition*, *129*, 241–255.

Schlesiger, M. I., Boublil, B. L., Hales, J. B., Leutgeb, J. K., & Leutgeb, S. (2018). Hippocampal global remapping can occur without input from the medial entorhinal cortex. *Cell Reports*, *22*, 3152–3159.

Skaggs, W. E., & McNaughton, B. L. (1998). Spatial firing properties of hippocampal CA1 populations in an environment containing two visually identical regions. *The Journal of Neuroscience*, *18*, 8455–8466.

Smith, D. M., & Bulkin, D. A. (2014). The form and function of hippocampal context representations. *Neuroscience and Biobehavioral Reviews*, *40C*, 52–61.

Smith, D. M., & Mizumori, S. J. Y. (2006). Learning-related development of context-specific neuronal responses to places and events: The hippocampal role in context processing. *The Journal of Neuroscience*, *26*, 3154–3163.

Solstad, T., Boccara, C. N., Kropff, E., Moser, M.-B., & Moser, E. I. (2008). Representation of geometric borders in the entorhinal cortex. *Science*, *322*, 1865–1868.

Spiers, H. J., Hayman, R. M. A., Jovalekic, A., Marozzi, E., & Jeffery, K. J. (2015). Place field repetition and purely local remapping in a multicompartment environment. *Cerebral Cortex*, *25*, 10–25.

Steyn-Ross, D. A., Steyn-Ross, M. L., Wilson, M. T., & Sleigh, J. W. (2010). Phase transitions in single neurons and neural populations: Critical slowing, anesthesia, and sleep cycles. In *Modeling phase transitions in the brain* (pp. 1–26). New York, NY: Springer.

Terrazas, A., Krause, M., Lipa, P., Gothard, K. M., Barnes, C. A., & McNaughton, B. L. (2005). Self-motion and the hippocampal spatial metric. *The Journal of Neuroscience*, *25*, 8085–8096.

Tkačik, G., Mora, T., Marre, O., Amodei, D., Palmer, S. E., Berry, M. J., & Bialek, W. (2015). Thermodynamics and signatures of criticality in a network of neurons. *Proceedings of the National Academy of Sciences of the United States of America*, *112*, 11508–11513.

Truccolo, W., Eden, U. T., Fellows, M. R., Donoghue, J. P., & Brown, E. N. (2004). A point process framework for relating neural spiking activity to spiking history, neural ensemble, and extrinsic covariate effects. *Journal of Neurophysiology*, *93*, 1074–1089.

Wills, T. J., Lever, C., Cacucci, F., Burgess, N., & O'Keefe, J. (2005). Attractor dynamics in the hippocampal representation of the local environment. *Science*, *308*, 873–876.

Wood, E. R., Dudchenko, P. A., Robitsek, R. J., & Eichenbaum, H. (2000). Hippocampal neurons encode information about different types of memory episodes occurring in the same location. *Neuron*, *27*, 623–633.

Zacks, J. M., Speer, N. K., Vettel, J. M., & Jacoby, L. L. (2006). Event understanding and memory in healthy aging and dementia of the Alzheimer type. *Psychology and Aging*, *21*, 466–482.

Zacks, J. M., & Swallow, K. M. (2007). Event Segmentation. *Current Directions in Psychological Science*, *16*, 80–84.

SUPPORTING INFORMATION

Additional supporting information may be found online in the Supporting Information section at the end of this article.

How to cite this article: Bulkin DA, Sinclair DG, Law LM, Smith DM. Hippocampal state transitions at the boundaries between trial epochs. *Hippocampus*. 2020;30:582–595. https://doi.org/10.1002/hipo.23180